Optical and electrochromic properties of DC magnetron sputter deposited tungsten oxide thin films at different electrolyte concentrations and vertex potentials for smart window applications

K. Naveen Kumar[1,2,*] , G. Nithya[2,3], Habibuddin Shaik[1,2], L. N. Chandrashekar[2,3], P. Aishwarya[2,3], and Amruth S. Pawar[2,4]

[1] *Department of Physics, Nitte Meenakshi Institute of Technology, Yelahanka, Bengaluru 560064, India*

[2] *Centre for Nano-Materials and MEMS, Nitte Meenakshi Institute of Technology, Yelahanka, Bengaluru 560064, India*

[3] *Department of Electronics and Communication, Nitte Meenakshi Institute of Technology, Yelahanka, Bengaluru 560064, India*

[4] *Department of VLSI Design, Manipal School of Information, Manipal 576104, Karnataka, India*

ABSTRACT

The main focus of this work is to analyze the electrochromic properties such as cyclic voltammetry, Diffusion co-efficient and Electrochemical properties like optical modulation, coloration efficiency, and the optical bandgap of colored and bleached states. The experiment was carried out by depositing WO_3 thin films on an FTO coated Glass substrate and carried out SEM characterization which showed a smooth surface and thickness of 500 nm, XRD for the structural characterization which revealed the amorphous nature, UV–vis Spectrometer for optical transmittance which showed 80% transmittance, EDS analysis shows that there are no impurities in the film grown and evidence the presence of W and O in the deposited film. An electrochemical analyzer was used to characterize the deposited film submerged in the electrolyte solution of different H_2SO_4 Molar concentrations of 0.2 M, 0.4 M, 0.6 M, 0.8 M, and 1 M with varied vertex potential sweeps from ± 0.6 to ± 1 V, through which it was observed that the highest cathodic peak current density is 16.32 mA/cm^2 for 1 M electrolyte solution for the vertex potential ± 1 V. And the optical band-gap for colored and bleached states is determined to be 3.04 eV and 3.294 eV, respectively, for 1 M H_2SO_4 electrolyte concentration. The highest coloration efficiency of 121.02 cm^2/C was seen in 0.8 M with vertex potential of − 0.6 to 0.6 V.

Address correspondence to E-mail: naveenkilari95@gmail.com

🙆 Springer

1 Introduction

The materials possessing electrochromic properties have grabbed researchers' attention to reduce the global challenges related to energy depletion. The electrochromic phenomenon has been observed when a low electric field is applied to some transition metal oxides, causing a new optical absorption band to emerge via the redox process and, as a result, color changes and back to its initial configuration when the electric field is removed because the redox process is reversible [1, 2]. There are several potential inorganic Electrochromic (EC) materials such as NiO [3], TiO$_2$ [4],WO$_3$ [5, 6] and V$_2$O$_5$ [7]. This work addresses the EC properties of WO$_3$ material which is an inorganic n-type semiconductor transition metal oxide that exhibits cathodic electrochromic behavior properties such as high reversible capacity, high optical modulation, good cyclic stability, and high-rate capability [8] which is researched extensively because of its wide bandgap range to 3 eV under Room Temperature (RT). When the negative and positive bias is applied to the host structure, they appear deep blue and colorless respectively. The electrochromic (EC) phenomena are considered to exemplify reversible optical characteristics under the application of voltage. The transition metal oxide's reflectance, absorbance, and transmittance can be altered via reversible electrochemical processes. Some of the deposition techniques that have been employed to deposit the WO$_3$ thin films are Hydrothermal method [9–12], pulsed laser deposition [13], electrospinning [14], chemical vapor deposition [15], RF & DC magnetron sputtering [16–22], Thermal evaporation [23], E-beam evaporation [24, 25], spin-coating [26], and many more.

Some of the potential applications where this transition metal oxide can be employed as an active sheath for gas sensors, humidity temperature sensors as well as for optical memories, flat panel displays, and filters [27]. It has the ability to switch its color for chromogenic applications under the application of electric field or potential, also can be used in energy-efficient smart windows, anti-glare mirrors, non-emissive mirrors, and many more [28]. The main reason behind the extensive research is that these materials are low-cost, reliable, simple operating mechanisms and can be coupled with micro-level devices. The cyclic voltammetry technique is used to investigate the redox reactions of species. A strategy that is employed to analyze the reaction pathways that include the transport of electrons by adjusting an electrode potential between two limits (called vertex potential) at a constant pace while monitoring the current that developed in the electrochemical cell. The main emphasis of this paper is to study the effect of change in electrolyte concentration and the vertex potential on electrochromic, and optical behavior of the DC magnetron sputtered tungsten oxide thin films.

2 Experimental setup

Tungsten oxide (WO$_3$) thin films were prepared on the FTO (Fluorine doped Tin Oxide) glass substrates by DC magnetron sputtering using tungsten (99.99% purity, 3-inch diameter) metal (W) as a target. The glass samples were ultrasonically cleaned by using soap solution, deionized water (DI), and acetone, which are dried with nitrogen gas. The magnetron sputtering system was initially evacuated to a base pressure of 3×10^{-6} mbar and working pressure of 1×10^{-2} mbar. The process parameters were specifically tailored at DC current of 100 mA (470 V), 25 sccm of Argon as a sputtering gas, and oxygen partial pressure of 8×10^{-4} mbar as reactive gas. The substrate to target distance was maintained at 9 cm. The duration of deposition was fixed to 20 min in RT and pre-sputtered the target for 10 min to remove the oxide layer and contaminants from the surface of the target. To study the characteristics of the deposited thin film, an aqueous electrolyte solution of 0.2, 0.4, 0.6, 0.8, and 1 M concentrations was prepared for 50 ml of DI water.

3 Results and discussions

3.1 Surface and structural analysis

Figure 1 illustrates the SEM and EDS spectra of WO$_3$ films. Figure 1a and b show the cross-sectional and morphology of WO$_3$ thin films deposited at room temperature as seen through a scanning electron microscope. The thickness was maintained at 500 nm. Figure 1c shows the compositional and elemental analysis of WO$_3$ thin films through EDS spectra. The energy range of the EDS spectra is 0 to 7 keV. The presence of distinctive peaks of W and O atoms is
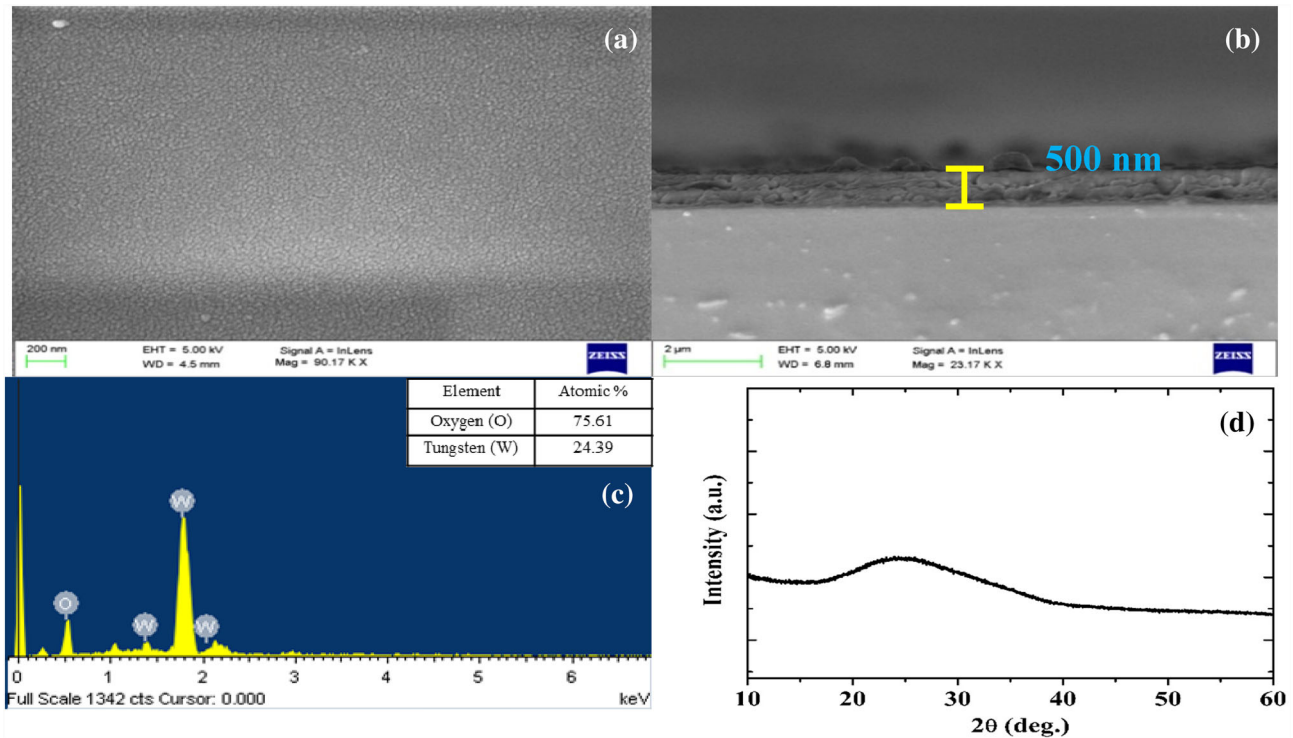
Fig. 1 SEM images of WO_3 films **a** top, **b** cross-sectional, **c** EDS Spectrum, and **d** XRD spectrum

evident in the presented spectra, but no other peaks can be seen. This indicates that no other contaminants are generated in the film and that the quality of WO_3 thin films deposited by DC Magnetron Sputtering is satisfactory [29]. The atomic percentage of W, and O elements are shown in inset of Fig. 1c. The atomic ratio of oxygen to tungsten was 3.10 and It indicated that the films formed nearly stoichiometric WO_3. Figure 1d shows the XRD pattern of RT-deposited samples. The broad peaks were observed in the XRD patron, which indicates the amorphous nature of the film because there was no applied temperature during the preparation process, so the tungsten ions reached the substrate surface with lower energy after combining with the oxygen ions. Mohamed et al. [30] reported that amorphous WO_3 films were deposited on unheated glass substrates by using DC magnetron sputtering.

3.2 Electrochemical studies

In order to investigate the electrochromic behavior of the deposited WO_3 thin films, we have used the SP300 potentiostat for cyclic voltammogram measurements which were performed using a programmable three-electrode setup. The coloring and bleaching kinetics of sputtered WO_3 thin films were investigated via periodic ion insertion or extraction during each scanning cycle [27]. The electrodes were immersed in the electrolyte (H_2SO_4) solution and consisted of a working electrode (FTO/WO_3 deposited thin film), a reference electrode (Hg/Hg_2Cl_2), and a counter electrode (Pt wire). When a negative bias is supplied to the working electrode, the intercalation of H^+ ions with the host matrix produces a deep blue color. In due course, under positive bias, H^+ ion deintercalation with the host matrix occurs, resulting in a shift from deep blue to transparent [31]. This research focuses on the impact of variation of concentration and vertex potential under a constant scan rate of 20 mV/s. The vertex potential is swept from ± 0.6 to ± 1 V with a step of 0.2 V, followed by the aqueous solution of H_2SO_4 solution, which is varied from 0.2 to 1 M with a step of 0.2 M change as depicted in Fig. 2.

As the vertex potential applied to the sputtered WO_3 thin film increases for 0.2 M, 0.4 M, 0.6 M, 0.8 M, and 1 M aqueous H_2SO_4 solution, the cathodic peak current density for ± 1 V is more than ± 0.8 V is greater than ± 0.6 V. For 0.2 M, 0.4 M, 0.6 M, 0.8 M, and 1 M aqueous H_2SO_4 electrolyte solution, the reduction peak current densities (mA/cm^2) for

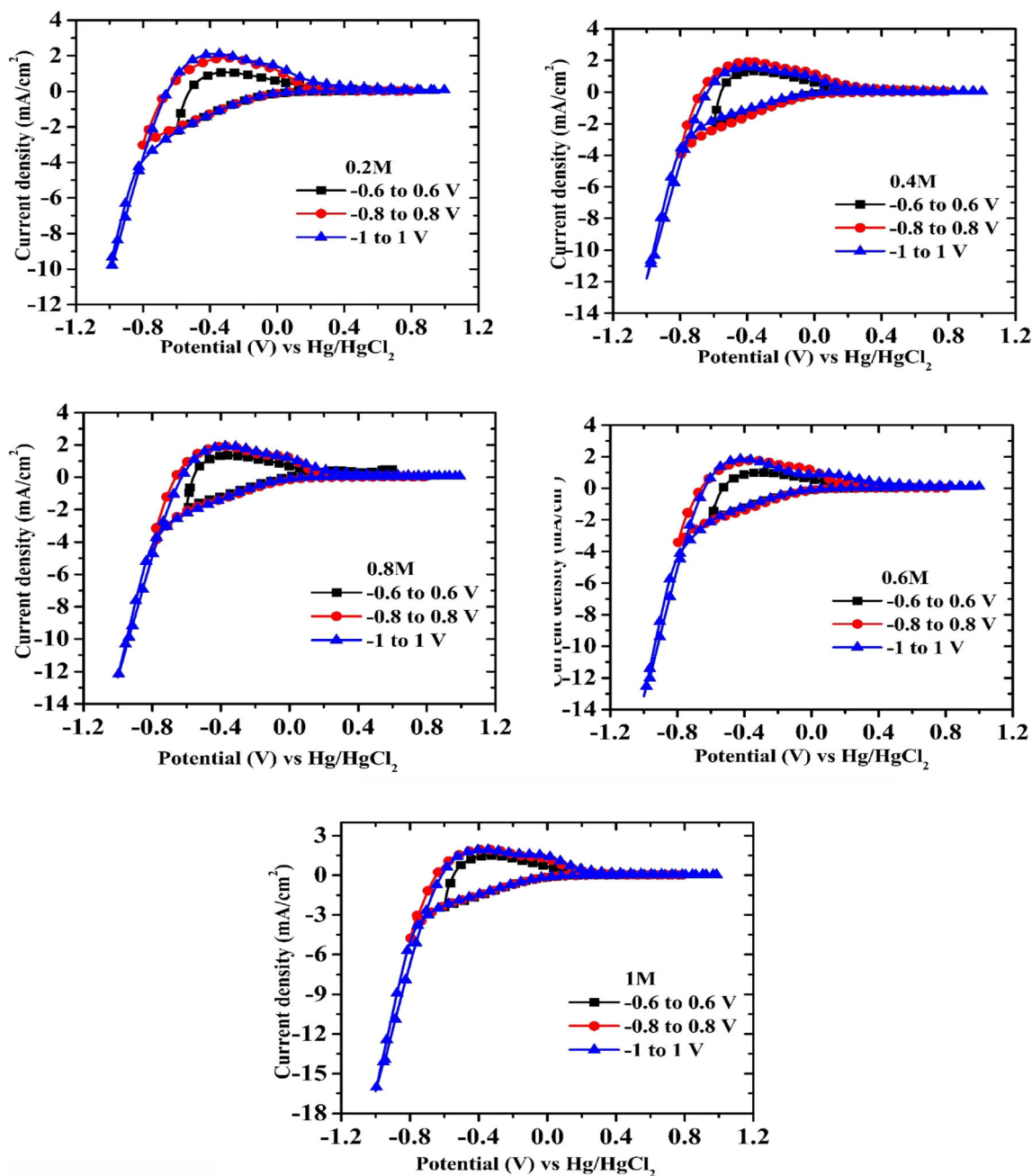**Fig. 2** Cyclic voltammograms for a particular electrolyte concentration for a varied vertex potential sweep

the listed vertex potentials going from ± 0.6 V and progressing to ± 1 V are recorded as $(-2.24, -3.01, -9.92)$, $(-2.07, -3.99, -11.79)$, $(-2, -3.66, -12.94)$, $(-1.94, -4.35, -12.35)$ and $(-2.41, -4.92, -16.32)$. The trend shown by the cyclic voltammetry characteristics in the below figures demonstrates that as the concentration of the electrolyte increases, so does the cathodic current density, indicating the number of ions intercalating into the WO_3 host matrix under the application of the vertex potential. Furthermore, the cathodic peak current density indicates the intensity of H^+ ion intercalation, and having a higher current density indicates faster intercalation. The charge storage capability of the film deposited is quantified based on the area under the cyclic voltammograms. As a reason, broad regions under the curve are more appropriate for Electrochromic applications [32].

From the below Cyclic Voltammograms (2), the area under the curve narrows when the vertex potential switches from ± 0.6 V, ± 0.8 V, and ± 1 V shown in Fig. 3. Furthermore, the number of ions participating in the redox process increases with increasing vertex potential and electrolyte

Fig. 3 Cyclic voltammograms for different electrolyte concentrations for a particular vertex potential sweep

concentration, indicating a higher cathodic peak current density.

The response time assessed from the trend of the current density change is one of the primary evaluation metrics for electrochromic performance. Figure 4a–e depicts the current density as a function of time with alternate constant vertex potentials acquired using an Electrochemical analyzer. The current density is mainly governed by the vertex potential, electrolyte molarity, and film area (2.25 cm^2). It is evident that as vertex potential increases, the reduction peak current density increases. The sample with the largest reduction peak current density was evaluated with a concentration of 1 M electrolyte. As the vertex potential is increased, the coloration of the films deposited will occur at a very minimal pace with cathodic polarization. For faster coloration of the deposited thin films, the concentration of the electrolyte should be more with the reduction in cathodic polarization [33].

Figure 5a and b show a comparative analysis featured for charge density vs Voltage and Molarity. As shown in Fig. 5 a, the charge density follows an exponential profile as the vertex potential increases for a given density of H$^+$ ions. Figure 5b illustrates that although the concentration of H$^+$ ions rises, the charge density at constant vertex potential sweep increases, signifying that the active charges participating in the electrochemical reaction increase in the host matrix.

Figure 6a–c features the Molarity v/s Diffusion coefficient for a vertex potential sweep from ± 0.6 to ± 1 V with a step of 0.2 V. The Diffusion coefficient of H$^+$ ions is calculated using the following Randles–Sevcik formula,

$$i_p = 2.69 \times 10^5 \times A \times n^{3/2} \times D^{1/2} \times C_o \times v^{1/2} \qquad (1)$$

where, A: area of active WO$_3$ film, n: is the number of electrons, D: is the diffusion Co-efficient mainly depends on the density of the film, i$_{P}$: is the peak current, v: is the scan rate, and C$_o$: is the electrolyte concentration [34].

From the above plots, it can be observed that with an increase in molarity, the Diffusion coefficient value reduces in both reductions as well as oxidation states. The large pullback in the diffusion current can be observed in the reduction state than in the oxidation state where the latter changes in a very small amount. This reduction of diffusion Coefficient with an increase in Molarity is due to an increase in ion
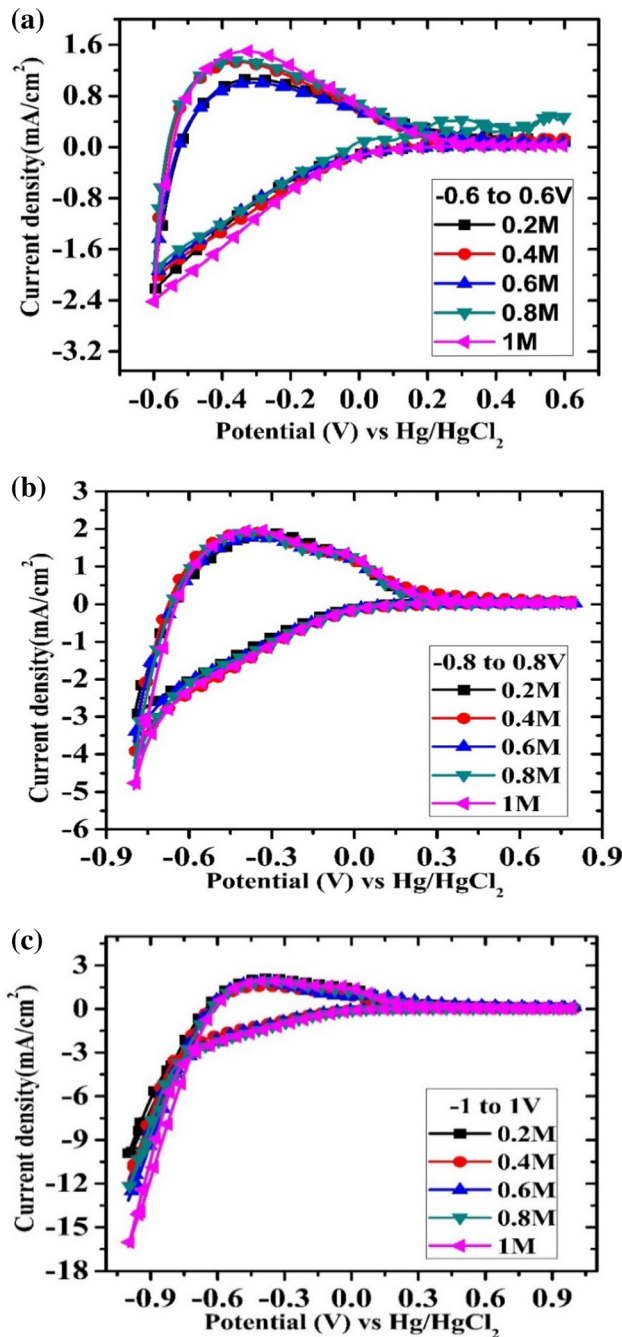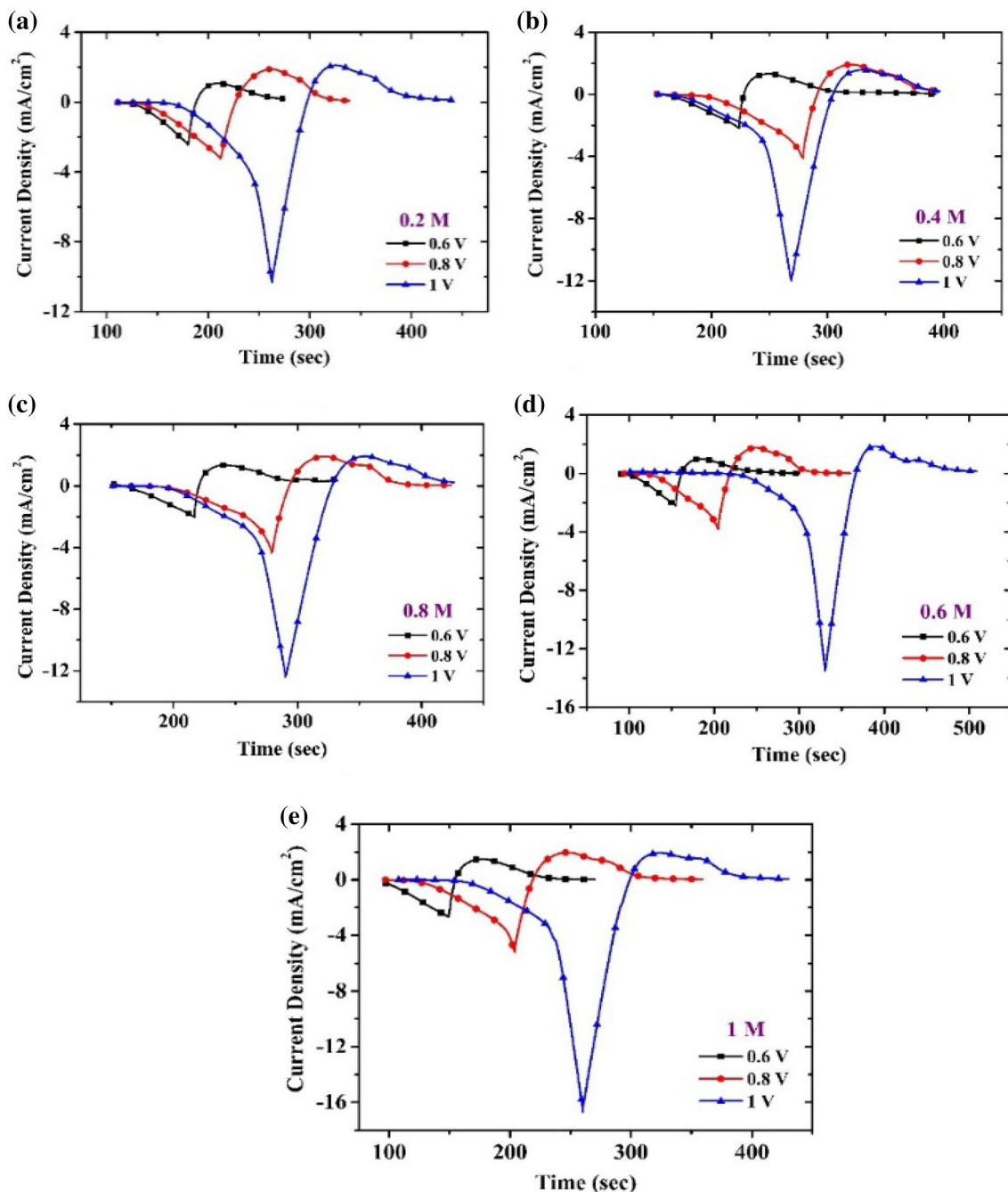
Fig. 4 current density vs time for different concentrations and concentrations of H^+

concentration which in turn reduces the accommodability of the ions. However, the highest value of diffusion coefficient in the reduction state and oxidation state is observed in 0.2 M H_2SO_4 solution when the vertex potential was swept from $\pm$ 1 V. The values of the diffusion coefficient at different H_2SO_4 molarity with all three vertex potential sweeps are tabulated below in Table 1.

Figure 7 depicts a plot of Vertex Potential versus Diffusion Coefficient for H_2SO_4 samples of varying molarity in both the Oxidation and Reduction phases. It was observed that the Diffusion Coefficient increases exponentially in the reduction state, but the changes are very minimal in the oxidation state.
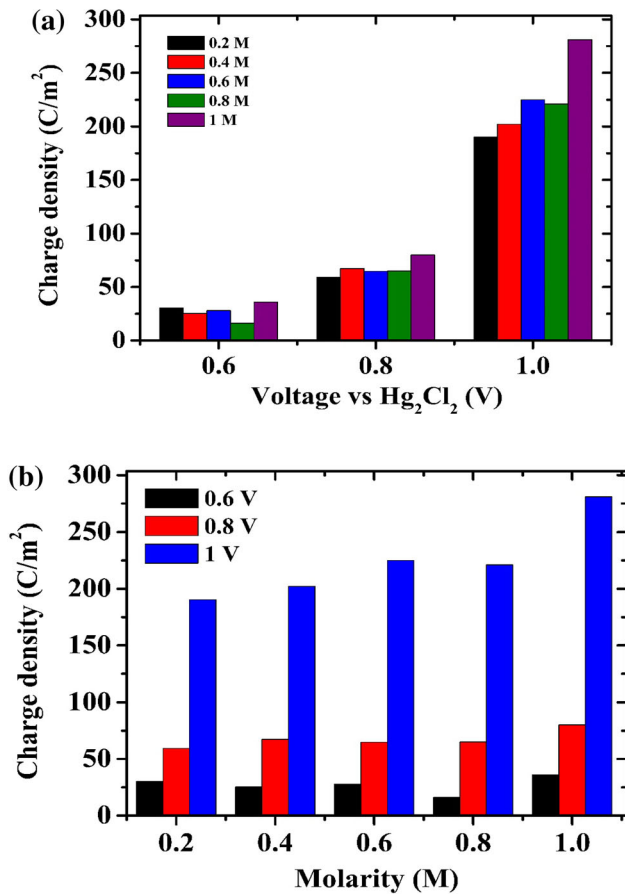
Fig. 5 **a** Charge density vs vertex potential for various molarities **b** Charge density vs Molarity for various vertex potential sweep

3.3 Electrochromic studies

The optical transmittance spectra for the DC sputtered tungsten oxide thin films have been studied using UV–Vis Spectrometer in the visible range. The transmittance for bleached and colored states acquired for different scanning potentials (0.6 V, 0.8 V, and 1 V) and different electrolyte concentrations (0.2–1 M) are shown in Fig. 8a–f. The observed values of transmittance at λ = 400 nm ranges from (13%–24%) for 0.6 V, (7%–15%) for 0.8 V, (3%–13%) for 1 V for coloured state and (60%–73%) for 0.6 V, (61%–71%) for 0.8 V and (45%–69%) for 1 V bleached state of WO_3 films. From this result, we can infer that as we increase the molarity of the electrolyte, the films are colored more densely due to the availability of more ions for intercalation (almost opaque) hence reducing the transmittance for the colored state; [35], [35]. There is no predominant effect on transmittance observed, by varying scanning potential for a
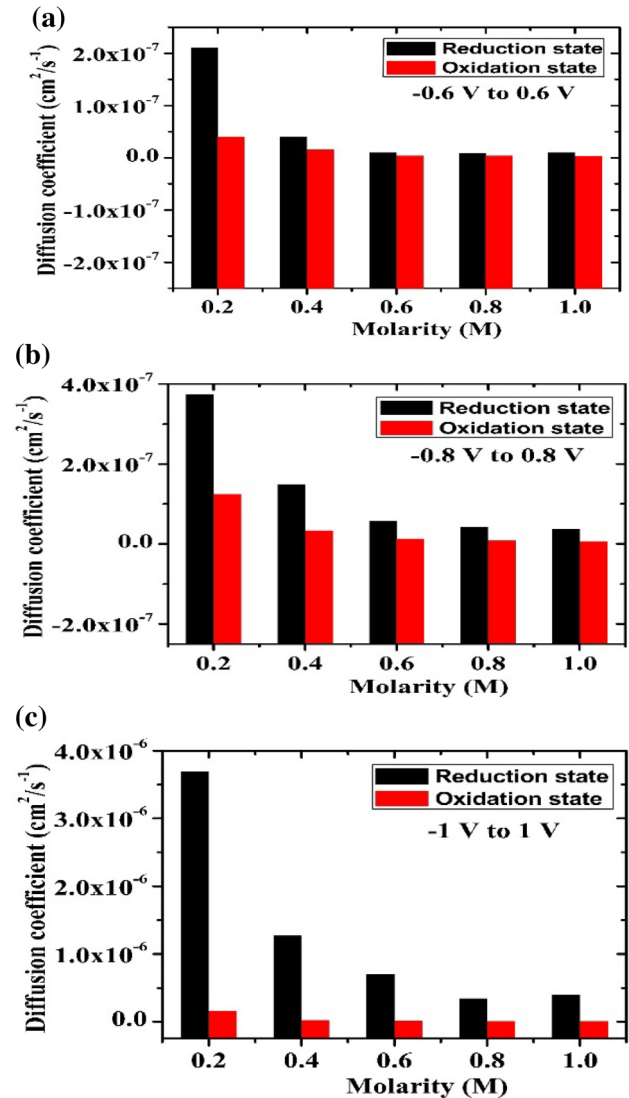

Fig. 6 Diffusion coefficient of H^+ ions vs molarity for different vertex potential sweep

particular concentration of electrolyte. Colored and bleached states of WO_3 thin films at different vertex potentials and electrolyte concentrations are shown in Fig. 8.

The optical energy band-gap of a cathodic semiconductive transition metal oxide 500 nm thick WO_3 samples is calculated as a function of absorption coefficient versus incident photon energy (eV) for different electrolyte concentrations and vertex potentials using the Tauc equation using Eq. (2).

$$(\alpha h v)^m = B(h - E_g) \tag{2}$$

where, α denotes the absorption coefficient of the material deposited, hv denotes the incident photon

Table 1 Diffusion coefficient of H^+ ions for different molarity and vertex potential sweep

Vertex potential sweep (V)	Molarity (M)	Diffusion coefficient (cm^2/s^{-1})	
		Reduction state	Oxidation state
± 0.6	0.2	2.105×10^{-7}	3.947×10^{-8}
	0.4	4.097×10^{-8}	1.534×10^{-8}
	0.6	9.984×10^{-9}	3.922×10^{-9}
	0.8	8.902×10^{-9}	4.018×10^{-9}
	1	9.984×10^{-9}	3.139×10^{-9}
± 0.8	0.2	3.733×10^{-7}	1.236×10^{-7}
	0.4	1.487×10^{-7}	3.239×10^{-8}
	0.6	5.679×10^{-8}	1.228×10^{-8}
	0.8	4.156×10^{-8}	7.986×10^{-9}
	1	3.719×10^{-8}	5.400×10^{-9}
± 1	0.2	3.687×10^{-6}	1.572×10^{-7}
	0.4	1.268×10^{-6}	2.140×10^{-8}
	0.6	7.049×10^{-7}	1.297×10^{-8}
	0.8	3.386×10^{-7}	8.060×10^{-9}
	1	3.908×10^{-7}	5.351×10^{-9}

energy in eV, B represents a proportionality constant, E_g denotes the optical band-gap energy in eV and m is 2 for direct and 0.5 for indirect [35].

The predicted band-gap trend for the oxygen-sputtered samples lies in the band of 2.358 to 3.294 eV and follows indirect transitions as gathered in Table 2. As the concentration of the aqueous electrolyte rises, so does the optical band-gap of the semiconductor deposited with the decrease in vertex potential sweep. The SPECORD 600 UV–Visible spectrometer (wavelength ranging from 200 to 1100 nm) was used to characterize the optical energy band gap. According to Guanguang Zhang et al., the optical energy band gap of the deposited WO_3 films in colored states is lower than that of their associated bleached state values. It is calculated that for 1 M H_2SO_4 electrolyte concentration, the optical band gap for the colored state is 3.04 eV and the bleached state is 3.294 eV [37].

Amongst the most crucial aspects of these transition metal oxides is their transmittance in both transparent and opaque phases, which is required for electrochromic applications. As an outcome, there is indeed a high optical modulation, ΔT, which is defined as the difference between the Transmittance of bleached and colored states [32]. Degradation in optical modulation of the host matrix can be flagged up over certain voltage cycles because the intercalated H^+ ions are not completely extracted from the film deposited. These trapped ions in the host matrix contribute to the deterioration of the electrochromic

performance of the material deposited. CV measurements were done and the bleached and colored switching attributes at 500, 550 and 600 nm for a varied vertex potential sweep from ± 0.6 V till ± 1 V with a step of 0.2 V were recorded.

The optical modulation is featured versus the wavelength for a constant vertex potential sweep with varying H_2SO_4 electrolyte concentrations. From below Fig. 9 it is evident that the optical modulation of the as-deposited film decreases with an increase in electrolyte concentration and the vertex potential sweep. For a wavelength of 550 nm, the estimated optical modulation for a 0.8 M electrolyte concentration, ± 0.6 V and ± 0.8 V vertex potential was found to be 84% and 80% respectively and 70% for 1 M electrolyte concentration and ± 1 V vertex potential.

The coloration efficiency is featured against the wavelength as depicted in Fig. 10 for deposited samples immersed in different molarity of H_2SO_4 solution. Coloration efficiency is calculated using the formula

$$CE \, or \, \eta = \Delta OD/(Qi/A) \tag{3}$$

where ΔOD: optical density, Q: charge, A: area of WO_3 film.

$$\Delta OD = \log(T_b/T_c) \tag{4}$$

where T_b and T_c are transmittances in bleached and colored states respectively [38] which were recorded using the UV Spectrometer. The graphs are plotted for wavelengths: 500 nm, 550 nm and 600 nm, and
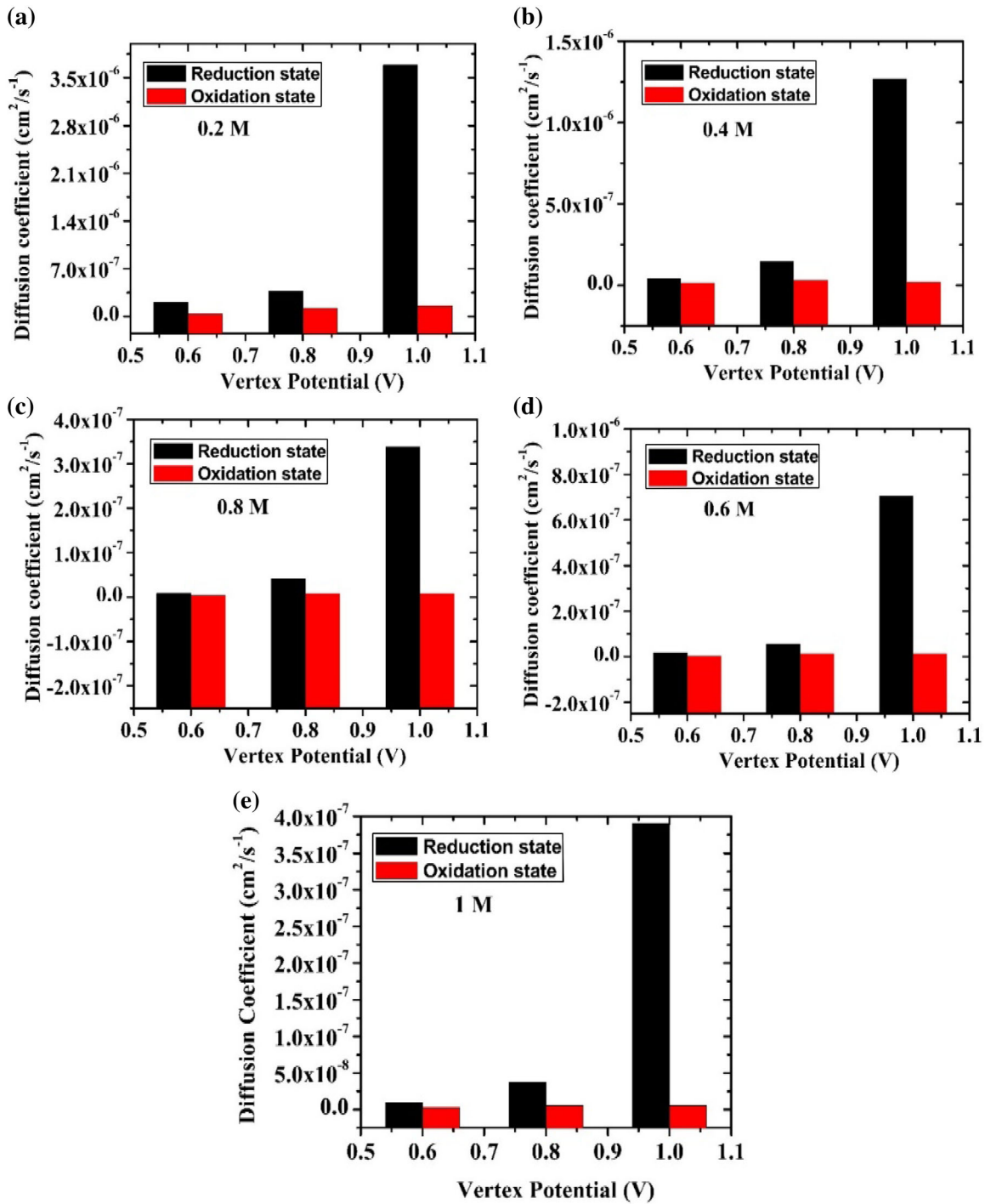
Fig. 7 Diffusion co-efficient vs Vertex potential for reduction and oxidation states

three vertex potential sweeps were considered for the study. In Fig. 8a, it can be clearly observed that the best coloration efficiency can be observed in the sample that was dipped in 0.8 M H_2SO_4 solution under $\pm$ 0.6 V vertex potential sweep as tabulated in Table 3. Similarly, in Fig. 10b and c, it can be observed that the best coloration efficiency is observed in 0.2 M H_2SO_4 solution for both $\pm$ 0.8 V and $\pm$ 1 V vertex potential sweeps and can be inferred using Tables 4 and 5.
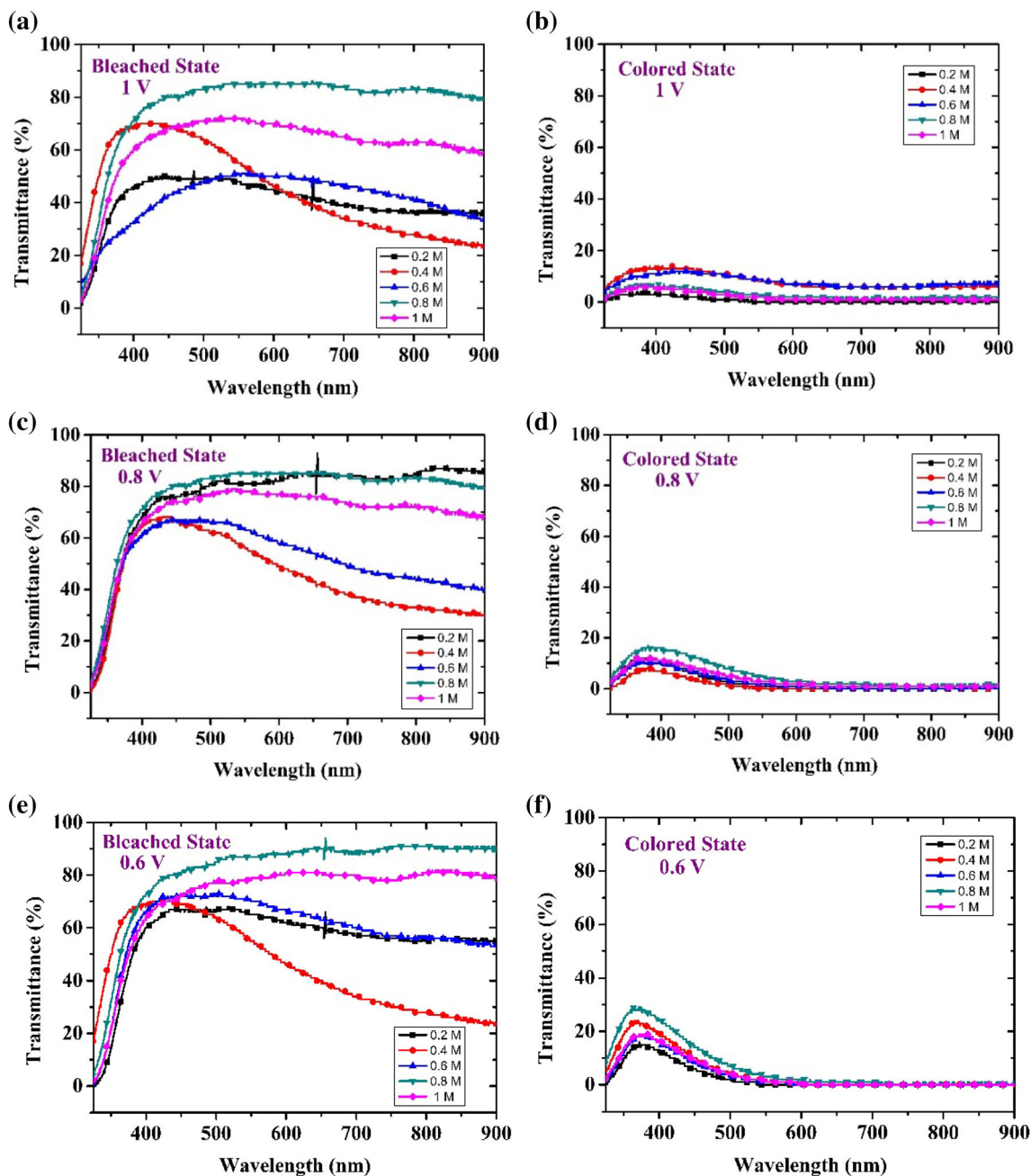
Fig. 8 Colored and bleached states of WO$_3$ thin films at different vertex potential and electrolyte concentration

Table 2 Bandgap for colored and bleached transmittance for different electrolyte concentrations and vertex potential sweep

Vertex potential	Transmittance state	Concentration (M)				
		0.2	0.4	0.6	0.8	1
− 0.6 V to 0.6 V	Coloured	2.964 eV	2.9918	3.03	3.031	3.04
	Bleached	3.0283	3.145	3.154	3.223	3.262
− 0.8 V to 0.8 V	Coloured	2.8264	2.8235	2.895	2.906	2.99
	Bleached	3.058	3.146	3.154	3.23	3.273
− 1 V to 1 V	Coloured	2.358	2.5826	2.649	2.83	2.935
	Bleached	3.08	3.153	3.23	3.25	3.294

(a)

(b)

(c)
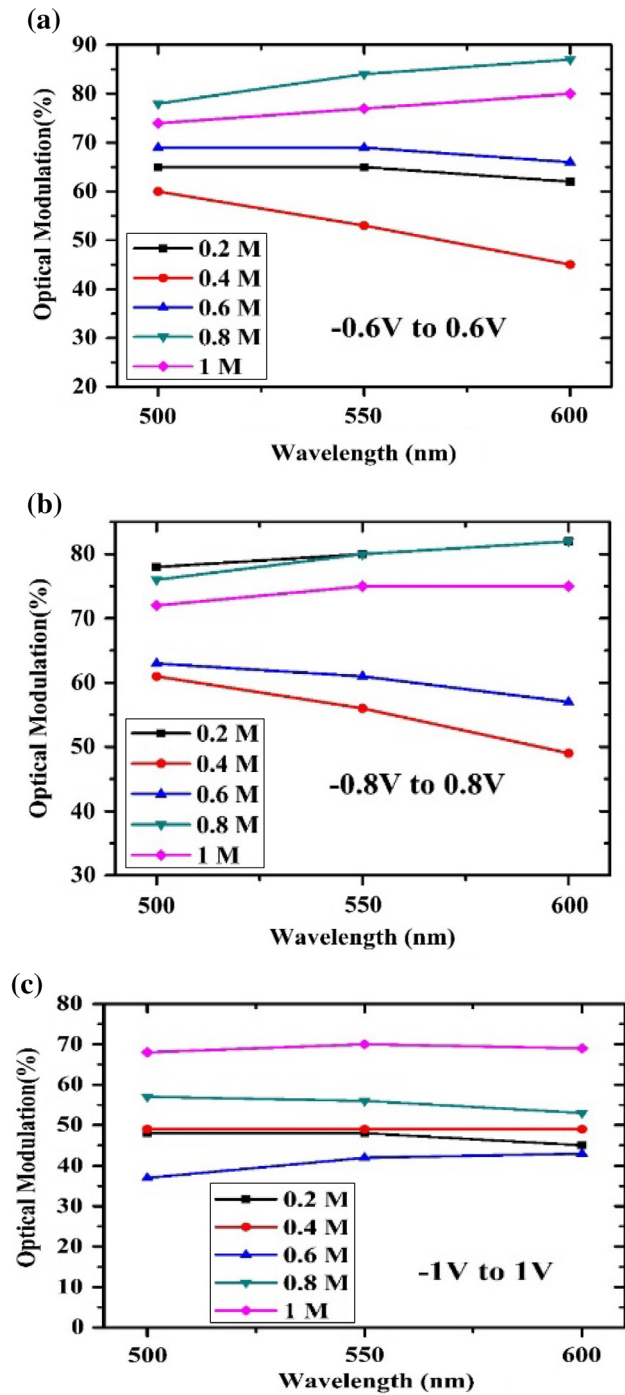
Fig. 9 Optical modulation versus the wavelength for a constant vertex potential sweep

(a)

(b)

(c)

Fig. 10 Coloration efficiency vs wavelength for different molarity and vertex potential sweep

4 Conclusion

In summary, the DC sputtered WO_3 thin films were deposited at RT and characterized for 0.2 M, 0.4 M, 0.6 M, 0.8 M, and 1 M electrolyte concentrations with varied vertex potential sweep from ± 0.6 to ± 1 V.
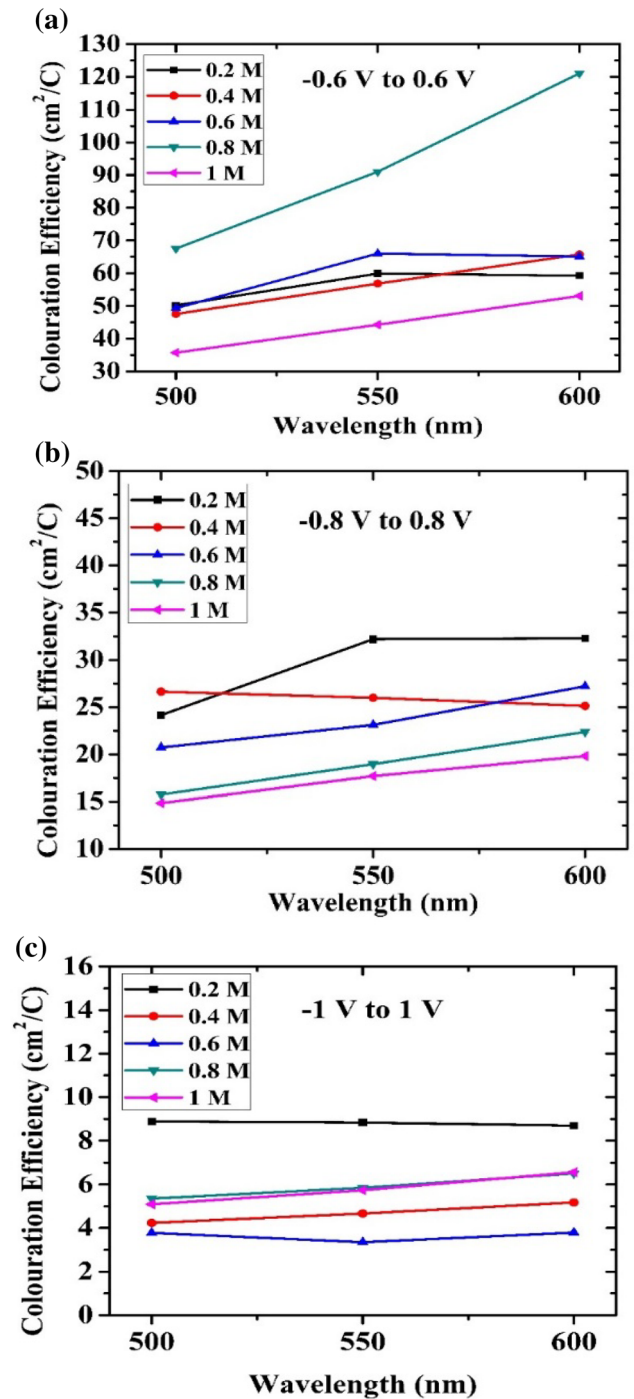
From the XRD analysis, it is evident that the deposited films are amorphous in nature due to the absence of a distinctive peak. EDS analysis shows that there are no impurities in the film grown and evidence of the presence of W and O in the deposited film. The highest reduction peak current density measured

Table 3 Coloration efficiency for a vertex potential sweep from ± 0.6 V

Vertex potential sweep (V)	Molarity (M)	Wavelength (nm)	T_b (%)	T_c (%)	CE (cm²/C)
± 0.6	0.2	500	66	2	50.22
		550	65	1	59.95
		600	62	1	59.28
	0.4	500	64	4	47.57
		550	55	2	56.86
		600	46	1	65.69
	0.6	500	72	3	49.35
		550	70	1	65.98
		600	66	1	65.06
	0.8	500	85	7	67.48
		550	87	3	91.02
		600	88	1	121.02
	1	500	77	4	35.73
		550	78	2	44.26
		600	81	1	53.09

Table 4 Coloration efficiency for a vertex potential sweep from ± 0.8 V

Vertex potential sweep (V)	Molarity (M)	Wavelength (nm)	T_b (%)	T_c (%)	CE (cm²/C)
± 0.8	0.2	500	81	3	24.14
		550	81	1	32.19
		600	82	1	32.28
	0.4	500	62	1	22.64
		550	56	1	25.98
		600	49	1	28.51
	0.6	500	66	3	20.71
		550	63	2	23.12
		600	58	1	27.21
	0.8	500	84	8	15.73
		550	85	5	18.95
		600	85	3	22.37
	1	500	77	5	14.83
		550	78	3	17.68
		600	77	2	19.81

using cyclic voltammetry was -16.32 mA/cm² for 1 M electrolyte solution for the vertex potential ± 1 V. From the current density vs time plot, it is noticed that as the vertex potential is increased, the coloring of the deposited thin film occurs at a slower rate, suggesting slower cathodic polarization. A comparison is drawn between the reduction peak current density and vertex potential and molarity, and it is found that as the vertex potential and molarity increase, the reduction peak current density follows an exponential trend, indicating that the number of H^+ ions participating in the redox reaction with the host matrix increases. The diffusion coefficient is found to be maximum for a vertex potential of ± 1 V and a concentration of 0.2 M electrolyte in the reduction state. The optical band gap for colored and bleached states is determined to be 3.04 eV and 3.294 eV, respectively, for 1 M H_2SO_4 electrolyte concentration. The estimated optical modulation for a wavelength of 550 nm and 0.8 M electrolyte concentration with ± 0.6 V and ± 0.8 V vertex potential w ± 1 V vertex potential. Coloration efficiency is optimum for a vertex potential sweep of ± 0.6 V at 0.8 M electrolyte concentration.

Table 5 Coloration efficiency for a vertex potential sweep from ± 1 V

Vertex Potential Sweep (V)	Molarity (M)	Wavelength (nm)	T_b (%)	T_c (%)	CE (cm^2/C)
± 1	0.2	500	49	1	8.88
		550	48	1	8.83
		600	45	1	8.68
	0.4	500	79	11	4.23
		550	79	9	4.66
		600	78	7	5.17
	0.6	500	78	11	3.78
		550	51	9	3.34
		600	50	7	3.79
	0.8	500	61	4	5.35
		550	59	3	5.85
		600	55	2	6.50
	1	500	81	3	5.09
		550	82	2	5.73
		600	70	1	6.56

Declarations

References

1. V.R. Buch, A.K. Chawla, S.K. Rawal, Review on electrochromic property for WO3 thin films using different deposition techniques. Mater. Today Proc. **3**(6), 1429–1437 (2016). https://doi.org/10.1016/j.matpr.2016.04.025

2. J. Gupta, H. Shaik, K.N. Kumar, A review on the prominence of porosity in tungsten oxide thin films for electrochromism. Ionics (Kiel) **27**(6), 2307–2334 (2021). https://doi.org/10.1007/s11581-021-04035-8

3. M.S. Wu, C.H. Yang, Electrochromic properties of intercrossing nickel oxide nanoflakes synthesized by electrochemically anodic deposition. Appl Phys Lett. (2007). https://doi.org/10.1063/12759270

4. A. Ghicov, S.P. Albu, J.M. Macak, P. Schmuki, High-contrast electrochromic switching using transparent lift-off layers of self-organized TiO_2 nanotubes. Small **4**(8), 1063–1066 (2008). https://doi.org/10.1002/smll.200701244

5. S.J. Yoo, J.W. Lim, Y.E. Sung, Y.H. Jung, H.G. Choi, D.K. Kim, Fast switchable electrochromic properties of tungsten oxide nanowire bundles. Appl. Phys. Lett. **90**(17), 88–91 (2007). https://doi.org/10.1063/1.2734395

6. J. Gutpa, H. Shaik, K. Naveen Kumar, S.A. Sattar, PVD techniques proffering avenues for fabrication of porous tungsten oxide (WO3) thin films: a review. Mater. Sci. Semicond Process. **143**, 106534 (2022). https://doi.org/10.1016/j.mssp.2022.106534

7. K.C. Cheng, F.R. Chen, J.J. Kai, V_2O_5 nanowires as a functional material for electrochromic device. Sol. Energy Mater. Sol. Cells **90**(7–8), 1156–1165 (2006). https://doi.org/10.1016/j.solmat.2005.07.006

8. Z. jie Xia et al., Enhanced electrochromic properties by improvement of crystallinity for sputtered WO3 film.

Coatings **10**(6), 1–11 (2020). https://doi.org/10.3390/COATINGS10060577

9. C.Y. Ng, K.A. Razak, A.A. Aziz, Z. Lockman, Formation of tungsten oxide nanorods by surfactant-assisted hydrothermal reaction. Int. Conf. Enabling Sci. Nanotechnol. (2012). https://doi.org/10.1109/ESciNano.2012.6149697

10. G.V. Ashok Reddy et al., Synthesis, characterizations, and electrochromic studies of WO3 coated CeO$_2$ nanorod thin films for smart window applications. Phys. B Condens. Matter. **647**, 414395 (2022). https://doi.org/10.1016/j.physb.2022.414395

11. G.V. Ashok Reddy et al., Effect of tungsten oxide thin films deposited on cerium oxide nano rods for electrochromic applications. Opt. Mater. (Amst) **134**, 113220 (2022). https://doi.org/10.1016/j.optmat.2022.113220

12. G.V. Ashok Reddy et al., Growth of cerium oxide nanorods by hydrothermal method and electrochromic properties of CeO$_2$/WO3 hybrid thin films for smart window applications. Mater. Today Proc. (2022). https://doi.org/10.1016/j.matpr.2022.11.316

13. M. E. M. A. Rougier, F. Portemer, A. Quede, Fs118 Candidate Selection Dossier. Appl. Surf. Sci. pp. 1–9 (1999)

14. Y. Fang et al., Thickness control in electrophoretic deposition of WO3 nanofiber thin films for solar water splitting. Mater. Sci. Eng. B **202**, 39–45 (2015). https://doi.org/10.1016/j.mseb.2015.09.005

15. E. Brescacin, M. Basato, E. Tondello, Amorphous WO3 films via chemical vapor deposition from metallorganic precursors containing phosphorus dopant. Chem. Mater. **11**(2), 314–323 (1999). https://doi.org/10.1021/cm980741n

16. K. Naveen Kumar et al., Glancing angle sputter deposited tungsten trioxide (WO3) thin films for electrochromic applications. Appl. Phys. A **128**(11), 1–8 (2022). https://doi.org/10.1007/s00339-022-06124-5

17. K. Naveen Kumar et al., Simulation and fabrication of tungsten oxide thin films for electrochromic applications. Phys. B Condens. Matter. **640**, 413932 (2022). https://doi.org/10.1016/j.physb.2022.413932

18. K. Naveen Kumar et al., Effect of annealing and oxygen partial pressure on the RF sputtered WO3 thin films for electrochromic applications. Mater. Today Proc. (2021). https://doi.org/10.1016/j.matpr.2021.11.185

19. K. Naveen Kumar, H. Shaik, V.M. Sathish, S. Abdul Sattar, On the bonding and electrochemical performance of Sputter deposited WO3 thin films. IOP Conf. Ser. Mater. Sci. Eng. (2020). https://doi.org/10.1088/1757-899X/872/1/012147

20. K.N. Kumar et al., Sputter deposited tungsten oxide thin films and nanopillars: electrochromic perspective. Mater. Chem. Phys. **278**, 125706 (2022). https://doi.org/10.1016/j.matchemphys.2022.125706

21. G.V. Ashok Reddy et al., Thickness dependent tungsten trioxide thin films deposited using DC magnetron sputtering for electrochromic applications. Mater. Today Proc. (2022). https://doi.org/10.1016/j.matpr.2022.11.134

22. V. Madhavi et al., Fabrication of porous 1D WO3 NRs and WO3/BiVO4 hetero junction photoanode for efficient photoelectrochemical water splitting". Mater. Chem. Phys. **274**, 125095 (2021). https://doi.org/10.1016/j.matchemphys.2021.125095

23. M.G. Hutchins, O. Abu-Alkhair, M.M. El-Nahass, K.A. El-Hady, Structural and optical characterisation of thermally evaporated tungsten trioxide (WO3) thin films. Mater. Chem. Phys. **98**(2–3), 401–405 (2006). https://doi.org/10.1016/j.matchemphys.2005.09.052

24. J. Gutpa, H. Shaik, K. Naveen Kumar, S.A. Sattar, Optimization of GLAD angle for E-Beam-fabricated tungsten oxide (WO3) thin films towards novel electrochromic behavior. J. Electron. Mater. (2022). https://doi.org/10.1007/s11664-022-10036-8

25. J. Gupta, H. Shaik, K.N. Kumar, S.A. Sattar, G.V.A. Reddy, Optimization of deposition rate for E-beam fabricated tungsten oxide thin films towards profound electrochromic applications. Appl. Phys. A Mater. Sci. Process. **128**(6), 1–15 (2022). https://doi.org/10.1007/s00339-022-05609-7

26. Z. Wang, X. Hu, Electrochromic properties of TiO$_2$-doped WO3 films spin-coated from Ti-stabilized peroxotungstic acid. Electrochim. Acta **46**(13–14), 1951–1956 (2001). https://doi.org/10.1016/S0013-4686(01)00384-X

27. M.B. Babu, K.V. Madhuri, Synthesis and electrochromic properties of nanocrystalline WO3 thin films. Phys. B Condens. Matter. (2020). https://doi.org/10.1016/j.physb.2020.412068

28. V. Hariharan et al., A review on tungsten oxide (WO3) and their derivatives for sensor applications to cite this version: HAL Id: hal-03093589 a review on tungsten oxide (WO 3) and their derivatives for sensor applications. Int. J. Adv. Sci. Eng. **5**(4), 1163–1168 (2021)

29. V. Madhavi, P. Kondaiah, O.M. Hussain, S. Uthanna, Structural, optical, and luminescence properties of reactive magnetron sputtered tungsten oxide thin films. ISRN Opt. **2012**, 1–8 (2012). https://doi.org/10.5402/2012/801468

30. S.H. Mohamed, H.A. Mohamed, H.A. Abd El Ghani, Development of structural and optical properties of WOx films upon increasing oxygen partial pressure during reactive sputtering. Phys. B Condens. Matter. **406**(4), 831–835 (2011). https://doi.org/10.1016/j.physb.2010.12.005

31. W. Kang, S. Park, H$_2$S Gas Sensing Properties of CuO Nanotubes. Appl. Sci. Converg. Technol. **23**(6), 392–397 (2014). https://doi.org/10.5757/asct.2014.23.6.392

32. B. Wen-Cheun Au, A. Tamang, D. Knipp, K.Y. Chan, Post-annealing effect on the electrochromic properties of WO3 films. Opt. Mater. (Amst) (2020). https://doi.org/10.1016/j.optmat.2020.110426

33. S.R. Bathe, P.S. Patil, WO3 thin films doped with Ru by facile chemical method with enhanced electrochromic properties for electrochromic window application. Mater. Sci. Eng. B Solid-State Mater. Adv. Technol. **257**, 114542 (2020). https://doi.org/10.1016/j.mseb.2020.114542

34. V. Madhavi, P. Kondaiah, O.M. Hussain, S. Uthanna, Structural, optical and electrochromic properties of RF magnetron sputtered WO3 thin films. Phys. B Condens. Matter. **454**, 141–147 (2014). https://doi.org/10.1016/j.physb.2014.07.029

35. I. Castro-Hurtado et al., Structural and optical properties of WO 3 sputtered thin films nanostructured by laser interference lithography. Appl. Surf. Sci. **276**, 229–235 (2013). https://doi.org/10.1016/j.apsusc.2013.03.072

36. A. Mehmood, A.A. Haidry, X. Long, X. Zhang, Influence of applied voltage on optimal performance and durability of tungsten and vanadium oxide co-sputtered thin films for electrochromic applications. Appl. Surf. Sci. (2021). https://doi.org/10.1016/j.apsusc.2020.147873

37. G. Zhang et al., Effects of annealing temperature on optical band gap of sol-gel tungsten trioxide films. Micromachines (2018). https://doi.org/10.3390/mi9080377

38. M. Meenakshi, R. Sivakumar, P. Perumal, C. Sanjeeviraja, Studies on electrochromic properties of RF sputtered vanadium oxide: tungsten oxide thin films. Mater. Today Proc. **3**(Icfmd 2015), S30–S39 (2016). https://doi.org/10.1016/j.matpr.2016.01.005